

## **TRAJECTORY DETERMINATION FOR PIPELINES USING AN INSPECTION ROBOT AND PIPELINE FEATURES**

**Shuo Zhang, Stevan Dubljevic**

*University of Alberta, Department of Chemical & Materials Engineering, T6G 2R3 Edmonton, AB, Canada*  
(✉ [shuo8@ualberta.ca](mailto:shuo8@ualberta.ca), +1 7804 923 111, [stevan.dubljevic@ualberta.ca](mailto:stevan.dubljevic@ualberta.ca))

### **Abstract**

Geographic trajectory of a pipeline is important information for pipeline maintenance and leak detection. Although accurate trajectory of a ground pipeline usually can be directly measured by using global positioning system technology, it is much difficult to determine trajectory for an underground pipeline where global positioning system signal cannot be received. In this paper, a new method to determine trajectory for an underground pipeline by using a pipeline inspection robot is proposed. The robot is equipped with a low-cost inertial measurement unit and odometers. The kinematic model, measurement model and error propagation model are established for estimating position, velocity and attitude of the robot. The path reconstruction algorithm for the robot is proposed to improve accuracy of trajectory determination based on pipeline features. The experiment is given to illustrate that the position errors of the proposed method are less than 40% of that of the standard extended Kalman filter.

**Keywords:** trajectory determination, pipeline inspection robot, pipeline feature, path reconstruction algorithm.

© 2021 Polish Academy of Sciences. All rights reserved

## **1. Introduction**

Pipeline system is the highest-efficient tool for gas and oil transportation compared to vehicular and/or railway transportation, ship and/or plane transportation. As pipelines must be free from the risk of degradation which could cause environmental hazards and potential threats to life, pipeline inspection is a crucial aspect of pipeline operations [1, 2]. For example, improper maintenance of a gas pipeline threatens property and life from explosion and fire resulting from pipeline leaks. Therefore, it is important to have a pipeline inspection system for reducing the likelihood and consequences of incidents where the geographic trajectory of the pipeline is the primary information for pipeline inspection [3, 4]. Pipeline inspection is completed by assessing and mitigating pipeline risks following the geographic trajectory of the pipeline. However, accurate geographic trajectories of some pipelines are unknown and have to be reconstructed for pipeline inspection.

Although the trajectory for above-ground pipelines can be directly reconstructed by *global positioning system* (GPS) technology, it is much difficult to determine the trajectory for an underground pipeline since GPS signal is blocked by the soil and/or the metal pipeline. A *pipeline inspection gauge* (PIG) travels inside the pipeline and can be used to obtain the trajectory for an underground pipeline using a carried location system [5–7]. The location system on a PIG is usually composed of an *inertial measurement unit* (IMU) and odometers to sense motion of the PIG [8,9]. Strapdown inertial navigation technology is applied to obtain the geographic trajectory of the pipeline where the odometers are applied for the velocity updates and *above-ground marks* (AGMs) located at every few kilometers are used for location coordinate updates [10–13]. In order to obtain accurate trajectory of a pipeline, a high-precision IMU, like a *fiber optic gyro* (FOG) based IMU, is usually used for the location system on the PIG [14–16]. However, the size of a high-precision IMU makes it difficult to use in a small-diameter pipeline and the price of a high-precision IMU extremely increases the cost for trajectory determination for a pipeline.

A *micro electro mechanical system* (MEMS) based IMU has a much smaller size and lower cost than a FOG based IMU and is tried to be used for trajectory determination for pipelines. Usually, a MEMS based IMU cannot provide high-precision inertial measurements and position errors are accumulated rapidly with travel distance of a PIG in a pipeline [18]. AGMs must be applied to timely correct the position of the PIG and make the accuracy of the position satisfy the requirement for trajectory determination [18–20]. Buildings, roads and rivers in a city usually make deployment of AMGs impossible and consequently, the accuracy of the position cannot fully meet the requirements without enough AGMs. In [21,22], pipeline junction detection using accelerometer measurements is proposed to improve the accuracy of the pipeline trajectory determination. However, in the case when the PIG moves slowly in the pipeline and there are no gaps on the inner surface of pipeline junctions, it is difficult to detect pipeline junctions by accelerometer measurements because there is almost no vibration happening when the PIG goes through the pipeline junctions.

In this paper, the pipeline inspection robot moves in a pipeline for reconstructing the trajectory of the pipeline. The pipeline inspection robot is equipped with a MEMS based IMU which is low cost and suitable for small-diameter pipelines. Sensor data from the IMU and the odometers are recorded. A new trajectory determination method for pipelines is proposed by using the data from the IMU and the odometers on the pipeline inspection robot. The kinematic model and measurement model of the robot are created. The error propagation model is derived for correcting position, velocity and attitude errors of the robot. Pipeline features are utilized to improve the accuracy of trajectory determination. The trajectory determination algorithm is given to obtain accurate pipeline trajectory. The main contributions of this paper are listed as follows: 1) the kinematic model, measurement model and error propagation model of the pipeline inspection robot are created; 2) the pipeline feature extraction method is proposed to determine the constraints on the attitude of the robot; 3) the new trajectory reconstruction algorithm is given to improve the accuracy of a trajectory based on pipeline features; 4) the experiment is conducted to show the advantage of the proposed trajectory determination method.

## 2. System modelling for the pipeline inspection robot

### 2.1. Pipeline inspection robot

The robot used for pipeline trajectory determination is shown in Fig. 1. The pipeline inspection robot is driven by motors. The odometers are used to measure velocity of the robot. The pipeline inspection robot can fit in pipelines with different diameters by adjusting the springs.

The minimum diameter for a pipeline in which the robot can be applied is 6 inches. The electronic system of the pipeline inspection robot is mainly composed of an IMU, a microcontroller, a memory card and batteries. Limited by the cost of a high-precision IMU, a MEMS based IMU (MPU6050) is used on the robot. The IMU with a three-axis accelerometer and a three-axis gyroscope provides inertial measurements of the robot. A magnetometer is not applied on the robot because magnetic field can be affected in underground metal pipelines. Sensor data are stored in the memory card. After the robot completes pipeline inspection, sensor data are uploaded to a computer and processed offline for trajectory determination.

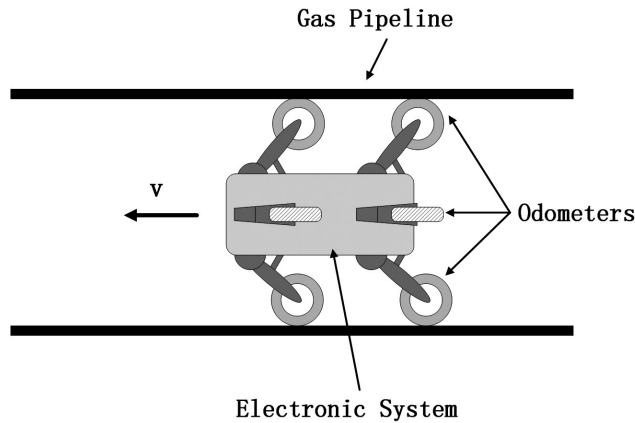


Fig. 1. Pipeline inspection robot.

## 2.2. Kinematic model and measurement model of the robot

The pipeline inspection robot travels in a gas pipeline and the path of the robot coincides with the pipeline trajectory. Therefore, the pipeline trajectory can be determined by reconstructing the path of the robot. Since, the robot is equipped with an IMU, the kinematic model of the pipeline inspection robot is created based on inertial navigation technique, where the differential equations are used to represent the position, velocity and attitude of the robot.

The frames used in the model are defined as follows:

The inertial frame (i-frame) is stationary with the origin at the center of mass of the Earth, z-axis pointing to the north pole and x-axis pointing to the vernal equinox.

The earth frame (e-frame) rotates along with the Earth with the origin at the center of mass of the Earth, z-axis pointing to the north pole and x-axis pointing to the intersection of the equatorial plan and the Greenwich meridian.

The navigation frame (n-frame) is on the surface of the Earth with the z-axis pointing downwards and the x-axis pointing to north.

The body fame (b-frame) is attached to the robot with the origin at the center of mass of the robot, the x-axis pointing forward and the z-axis pointing upwards. The frame of the IMU coincides with the body frame.

The position of the pipeline inspection robot is expressed by the latitude , the longitude and altitude . The velocity of the robot in the n-frame with respect to the e-frame is expressed by  $v^n = [v_N \ v_E \ v_D]^T$  where  $v_N$ ,  $v_E$  and  $v_D$  are the velocity components in the north, east and

down directions, respectively. The rate of change of the position is

$$\begin{aligned}\dot{\phi} &= \frac{v_N}{R_\phi + h}, \\ \dot{\lambda} &= \frac{v_E}{(R_\lambda + h) \cos \phi}, \\ \dot{h} &= -v_D,\end{aligned}\tag{1}$$

where  $R_\phi$  is the meridian radius of the Earth,  $R_\lambda$  is the normal radius of the Earth.

The rate of change of the velocity is given by [23]

$$\begin{aligned}\dot{v}_N &= -\left[\frac{v_E}{(R_\lambda + h) \cos \phi} + 2\omega_e\right]v_E \sin \phi + \frac{v_N v_D}{R_\phi + h} + f_N, \\ \dot{v}_E &= \left[\frac{v_E}{(R_\lambda + h) \cos \phi} + 2\omega_e\right]v_N \sin \phi + \frac{v_N v_D}{R_\lambda + h} + 2\omega_e v_D \cos \phi + f_E, \\ \dot{v}_D &= -\frac{v_E^2}{R_\lambda + h} - \frac{v_D^2}{R_\phi + h} - 2\omega_e v_E \cos \phi + g + f_D,\end{aligned}\tag{2}$$

where  $\omega_e$  is the angular rate of the Earth,  $g$  is the gravitational acceleration. The output of the three-axis accelerometer is called specific force  $f^b$  in the b-frame. The specific force  $f^n = [f_N \ f_E \ f_D]^T$  is the specific force  $f^b$  expressed in the n-frame obtained by coordinate transformation as follow:

$$f^n = R_b^n f^b,\tag{3}$$

where  $R_b^n$  is the rotation matrix.

The attitude quaternion is used to represent the attitude of the pipeline inspection robot. The attitude quaternion  $q$  is a four-parameter vector defined as  $q = [\rho^T \ q_4]^T$  with  $\rho = [q_1 \ q_2 \ q_3]^T$ .

The attitude quaternion  $q$  relates to the rotation matrix  $R_n^b$  by

$$R_n^b(q) = (q_4^2 - \|\rho\|^2)I_3 + 2\rho\rho^T - 2q_4[\rho \times],\tag{4}$$

where  $[\rho \times]$  is a skew symmetric matrix given by

$$[\rho \times] = \begin{bmatrix} 0 & -q_3 & q_2 \\ q_3 & 0 & -q_1 \\ -q_2 & q_1 & 0 \end{bmatrix}.\tag{5}$$

The rate of change of the attitude is given by

$$\dot{q} = \frac{1}{2}\Xi(q) \omega_{bn}^b\tag{6}$$

with

$$\Xi(q) = \begin{bmatrix} q_4 I_3 + [\rho \times] \\ -\rho^T \end{bmatrix},\tag{7}$$

where  $\omega_{bn}^b$  is the angular rate of the b-frame with respect to the n-frame expressed in the b-frame calculated as

$$\omega_{bn}^b = \omega_{bi}^b - \mathbf{R}_n^b(\mathbf{q}) \begin{bmatrix} \omega_e \cos \phi + \frac{v_E}{R_\lambda + h} \\ -\frac{v_N}{R_\phi + h} \\ -\omega_e \sin \phi - \frac{v_E \tan \phi}{R_\lambda + h} \end{bmatrix}. \quad (8)$$

Combining (1), (2) and (6), the kinematic model of the pipeline inspection robot is established.

The odometer measures the velocity of the robot in the b-frame, which is related to the velocity in the n-frame by the rotation matrix  $\mathbf{R}_n^b$ . The measurement model of the robot is given by

$$\tilde{\mathbf{v}}_{od}^b = \begin{bmatrix} \tilde{v}_{od} \\ 0 \\ 0 \end{bmatrix} = \mathbf{R}_n^b \begin{bmatrix} v_N \\ v_E \\ v_D \end{bmatrix} + \mathbf{v}, \quad (9)$$

where  $\tilde{v}_{od}$  is the velocity measured by the odometer,  $\mathbf{v}$  is zero-mean Gaussian white noise with the covariance  $\mathbf{R} = \sigma_{od}^2 \mathbf{I}_3$ .

### 2.3. Error propagation model

If true values of the angular rate and specific force are exactly known, the accurate position, velocity and attitude can be obtained based on the kinematic model, and then high-precision path reconstruction is achieved. Unfortunately, it is inevitable that there are measurement errors in the data of angular rate and specific force, especially for a low-cost IMU [24]. Position, velocity and attitude errors of the robot are rapidly accumulated with error propagation in the kinematic model. The error propagation model is introduced in this section for correcting position, velocity and attitude of the robot.

Considering measurement errors, the three-axis gyroscope measurement model is given by

$$\begin{aligned} \tilde{\omega}_{bi}^b &= \omega_{bi}^b + \boldsymbol{\beta}_g + \boldsymbol{\eta}_{gv}, \\ \dot{\boldsymbol{\beta}}_g &= \boldsymbol{\eta}_{gu}, \end{aligned} \quad (10)$$

where  $\boldsymbol{\beta}_g$  is the gyroscope bias,  $\boldsymbol{\eta}_{gv}$  and  $\boldsymbol{\eta}_{gu}$  are zero-mean Gaussian white noises with the covariance matrices given by  $\sigma_{gv}^2 \mathbf{I}_3$  and  $\sigma_{gu}^2 \mathbf{I}_3$ , respectively.

The accelerometer measurement model is given by

$$\begin{aligned} \tilde{\mathbf{f}}^b &= \mathbf{f}^b + \boldsymbol{\beta}_a + \boldsymbol{\eta}_{av}, \\ \dot{\boldsymbol{\beta}}_a &= \boldsymbol{\eta}_{au}, \end{aligned} \quad (11)$$

where  $\boldsymbol{\beta}_a$  is the accelerometer bias,  $\boldsymbol{\eta}_{av}$  and  $\boldsymbol{\eta}_{au}$  are zero-mean Gaussian white noises with the covariance matrices given by  $\sigma_{av}^2 \mathbf{I}_3$  and  $\sigma_{au}^2 \mathbf{I}_3$ , respectively.

Since the kinematic model of the robot is nonlinear, linearization is required for deriving the error propagation model. First, we define state error vector  $\delta \mathbf{x} = [\delta \alpha^T \ \delta \mathbf{p}^T \ (\delta \mathbf{v}^n)^T \ \delta \boldsymbol{\beta}_g^T \ \delta \boldsymbol{\beta}_a^T]^T$  and the process noise vector  $\mathbf{w} = [\boldsymbol{\eta}_{gv}^T \ \boldsymbol{\eta}_{gu}^T \ \boldsymbol{\eta}_{av}^T \ \boldsymbol{\eta}_{au}^T]^T$ , where  $\mathbf{p} = [\phi \ \lambda \ h]^T$ ,  $\mathbf{v}^n = [v_N \ v_E \ v_D]^T$ ,  $\delta \alpha$  represents the attitude error. The process noise covariance is  $\mathbf{Q} = \text{diag}(\sigma_{gv}^2 \mathbf{I}_3, \sigma_{gu}^2 \mathbf{I}_3, \sigma_{av}^2 \mathbf{I}_3, \sigma_{au}^2 \mathbf{I}_3)$ .

Substituting (10) and (11) into (2) and (6), the error propagation model is obtained by using the Taylor expansion.

$$\begin{aligned} \delta \dot{\mathbf{x}} &= \mathbf{F} \delta \mathbf{x} + \mathbf{G} \mathbf{w}, \\ \delta \mathbf{v}_{od}^b &= \mathbf{H} \delta \mathbf{x} + \mathbf{v}, \end{aligned} \quad (12)$$

where

$$\mathbf{F} \approx \begin{bmatrix} -[(\tilde{\omega}_{bi}^b - \hat{\beta}_g) \times] & \mathbf{F}_{12} & \mathbf{F}_{13} & -\mathbf{I}_3 & \mathbf{0}_3 \\ \mathbf{0}_3 & \mathbf{F}_{22} & \mathbf{F}_{23} & \mathbf{0}_3 & \mathbf{0}_3 \\ -\mathbf{R}_b^n(\hat{\mathbf{q}}) [(\tilde{\mathbf{f}} - \hat{\beta}_a) \times] & \mathbf{F}_{32} & \mathbf{F}_{33} & \mathbf{0}_3 & -\mathbf{R}_b^n(\hat{\mathbf{q}}) \\ \mathbf{0}_3 & \mathbf{0}_3 & \mathbf{0}_3 & \mathbf{0}_3 & \mathbf{0}_3 \\ \mathbf{0}_3 & \mathbf{0}_3 & \mathbf{0}_3 & \mathbf{0}_3 & \mathbf{0}_3 \end{bmatrix}, \quad (13)$$

$$\mathbf{F}_{12} \approx -\mathbf{R}_n^b(\hat{\mathbf{q}}) \begin{bmatrix} -\omega_e \sin \phi & 0 & 0 \\ 0 & 0 & 0 \\ -\omega_e \cos \phi - \frac{v_E \sec^2 \phi}{R_\lambda} & 0 & 0 \end{bmatrix}, \quad \mathbf{F}_{13} = -\mathbf{R}_n^b(\hat{\mathbf{q}}) \begin{bmatrix} 0 & \frac{1}{R_\lambda+h} & 0 \\ -\frac{1}{R_\phi+h} & 0 & 0 \\ 0 & -\frac{\tan \phi}{R_\lambda+h} & 0 \end{bmatrix}, \quad (14)$$

$$\mathbf{F}_{22} \approx \begin{bmatrix} 0 & 0 & 0 \\ \frac{v_E \sec \phi \tan \phi}{R_\lambda+h} & 0 & 0 \\ 0 & 0 & 0 \end{bmatrix}, \quad \mathbf{F}_{23} = \begin{bmatrix} \frac{1}{R_\phi+h} & 0 & 0 \\ 0 & \frac{\sec \phi}{R_\lambda+h} & 0 \\ 0 & 0 & -1 \end{bmatrix}, \quad (15)$$

$$\mathbf{F}_{32} \approx \begin{bmatrix} -\frac{v_E^2 \sec^2 \phi}{R_\lambda+h} - 2\omega_e v_E \cos \phi & 0 & 0 \\ \frac{v_E v_N \sec^2 \phi}{R_\lambda+h} + 2\omega_e (v_N \cos \phi - v_D \sin \phi) & 0 & 0 \\ 2\omega_e v_E \sin \phi + 0.103718 \sin \phi \cos \phi & 0 & -3.0877 \times 10^{-6} \end{bmatrix}, \quad (16)$$

$$\mathbf{F}_{33} = \begin{bmatrix} \frac{v_D}{R_\phi+h} & -\frac{2v_E \tan \phi}{R_\lambda+h} + 2\omega_e \sin \phi & \frac{v_N}{R_\phi+h} \\ \frac{2v_E \tan \phi}{R_\lambda+h} + 2\omega_e \sin \phi & \frac{v_D + v_N \tan \phi}{R_\lambda+h} & \frac{v_E}{R_\lambda+h} + 2\omega_e \cos \phi \\ -\frac{2v_N}{R_\phi+h} & -\frac{2v_E}{R_\lambda+h} - 2\omega_e \cos \phi & 0 \end{bmatrix}, \quad (17)$$

$$\mathbf{G} = \begin{bmatrix} -\mathbf{I}_3 & \mathbf{0}_3 & \mathbf{0}_3 & \mathbf{0}_3 \\ \mathbf{0}_3 & \mathbf{0}_3 & \mathbf{0}_3 & \mathbf{0}_3 \\ \mathbf{0}_3 & \mathbf{0}_3 & -\mathbf{R}_b^n(\hat{\mathbf{q}}) & \mathbf{0}_3 \\ \mathbf{0}_3 & \mathbf{I}_3 & \mathbf{0}_3 & \mathbf{0}_3 \\ \mathbf{0}_3 & \mathbf{0}_3 & \mathbf{0}_3 & \mathbf{I}_3 \end{bmatrix}, \quad (18)$$

$$\mathbf{H} = \left[ \left[ (\mathbf{R}_n^b(\hat{\mathbf{q}}) \hat{\mathbf{v}}^n) \times \right] \quad \mathbf{0}_3 \quad \mathbf{R}_n^b(\hat{\mathbf{q}}) \quad \mathbf{0}_{3 \times 6} \right], \quad (19)$$

$$\delta \mathbf{v}_{od}^b = \tilde{\mathbf{v}}_{od}^b - \mathbf{R}_n^b(\hat{\mathbf{q}}) \hat{\mathbf{v}}^n. \quad (20)$$

There are some terms in (13) containing expressions where velocities are divided by the square of the Earth's radius. Since the pipeline inspection robot moves with low velocity, these terms are relatively minor and can be safely ignored.

Based on (12), the discrete-time error propagation model is given by

$$\begin{aligned} \delta \mathbf{x}_{k+1} &= \mathbf{A}_k \delta \mathbf{x}_k + \mathbf{G}_k \mathbf{w}_k, \\ \delta \mathbf{v}_{od,k}^b &= \mathbf{H}_k \delta \mathbf{x}_k + \mathbf{v}_k, \end{aligned} \quad (21)$$

where  $\mathbf{A}_k = \mathbf{I}_{15} + \mathbf{F}_k T_s$  and  $T_s$  is the sampling time. The covariance of the process noise  $\mathbf{w}_k$  is  $\mathbf{Q} T_s$ .

It can be seen in (21) that the state error is caused by process noise  $\mathbf{w}_k$  which contains the characteristics of the measurement errors from the gyroscope and the accelerometer. The biases and noises of the gyroscope and the accelerometer in (10) and (11) are considered to establish the error propagation model. Since sensor outputs  $\tilde{\omega}_{bi}^b$  and  $\tilde{\mathbf{f}}^b$  are parameters in the kinematic model of the pipeline inspection robot, the biases and noises of the sensors are introduced into the kinematic model. The error propagation model (21) describes the way that the sensor errors propagate in the kinematic model. The velocities read from the odometers are used as the observation and the measurement error  $\mathbf{v}_k$  of the odometer is in the error model of the measurement equation in (21). The state error increases due to the errors of the gyroscope and the accelerometer. Therefore, the filtering algorithm is applied to correct the state estimate.

### 3. Path reconstruction for the pipeline inspection robot

Pipeline trajectory determination is achieved by reconstructing the path of the pipeline inspection robot. Based on the kinematic model, measurement model and error propagation model, the *extended Kalman filter* (EKF) can be applied to estimate the system state including the position, velocity and attitude of the robot. However, since the low-cost IMU cannot provide high-precision inertial measurements, the accuracy of the state estimation deteriorates even though the odometer measurement is used in the EKF for state error correction. In this section, features of pipelines are introduced as additional information for improving accuracy of path reconstruction for the robot.

#### 3.1. Attitude constraints based on the pipeline features

The following pipeline features are considered in this paper: a) the pipeline system is composed of several sections of straight pipelines; b) most pipelines are in horizontal planes; c) pipe elbows have standard angles. The method based on a sliding window is proposed to extract the pipeline features above using inaccurate attitude estimates obtained by the EKF. The size  $L$  of the sliding window  $\{k-L+1, k\}$  represents a short time interval and is chosen based on the sampling time and the velocity of the robot.

Given the inaccurate attitude quaternion estimate  $\hat{\mathbf{q}}$  obtained by the EKF, the attitude matrix can be calculated by (4) and the Euler angle  $\hat{\boldsymbol{\alpha}} = [\hat{\alpha}_1 \quad \hat{\alpha}_2 \quad \hat{\alpha}_3]^T$  is given by

$$\begin{aligned} \hat{\alpha}_1 &= a \tan 2 \left( \mathbf{R}_n^b(2, 3), \mathbf{R}_n^b(3, 3) \right), \\ \hat{\alpha}_2 &= -a \sin \left( \mathbf{R}_n^b(1, 3) \right), \\ \hat{\alpha}_3 &= a \tan 2 \left( \mathbf{R}_n^b(1, 2), \mathbf{R}_n^b(1, 1) \right), \end{aligned} \quad (22)$$

where  $R_n^b(i, j)$  is the  $(i, j)$  element of  $R_n^b(\hat{q})$ ,  $\hat{\alpha}_1$ ,  $\hat{\alpha}_2$  and  $\hat{\alpha}_3$  are the roll, pitch and yaw angles, respectively. Based on the Euler angle estimates  $\hat{\alpha}_{k-L+1}$  and  $\hat{\alpha}_k$  at the time  $k-L+1$  and  $k$ , the pipeline features are extracted and, accordingly, the constraints on the attitude of the robot caused by the pipeline features are determined as follows:

If  $|\hat{\alpha}_{2,k}| < \varepsilon$  with  $\varepsilon$  being positive, the robot is in a horizontal pipeline at the time  $k$  and the constraint for the pitch angle of the robot satisfies

$$\alpha_{2,k} = 0. \quad (23)$$

Similarly, if  $|\hat{\alpha}_{2,k}| - \pi/2 < \varepsilon$ , the robot is in a vertical pipeline at that moment and we have

$$\alpha_{2,k} = \text{sgn}(\hat{\alpha}_{2,k}) \pi/2, \quad (24)$$

where  $\text{sgn}$  is the sign function.

If  $|\hat{\alpha}_{2,k} - \hat{\alpha}_{2,k-L+1}| < \varepsilon$  and  $|\hat{\alpha}_{3,k} - \hat{\alpha}_{3,k-L+1}| < \varepsilon$ , the robot is in a straight pipeline during the time in the sliding window  $\{k-L+1, k\}$ . Since the pitch and yaw angles of the robot are constant in a straight pipeline, we have the following constraints:

$$\begin{aligned} \alpha_{2,i} &= \alpha_{2,k-L+1}, \\ \alpha_{3,i} &= \alpha_{3,k-L+1}, \quad i = k-L+2, \dots, k. \end{aligned} \quad (25)$$

If  $|\hat{\alpha}_{3,k} - \hat{\alpha}_{3,k-L+1}| - \theta^* < \varepsilon$  for  $k \in [k_1, k_1+M]$ , where  $M$  is a positive integer chosen based on the sampling time and the velocity of the robot, it indicates that the path of the robot becomes a straight line again at the time  $k_1$  after a turning through  $\theta^*$  at a pipe elbow and  $\theta^*$  is the standard angle of the pipe elbow. We have the following constraints:

$$\begin{aligned} \alpha_{3,k_1} &= \alpha_{3,k_1-L+1} + \text{sgn}(\hat{\alpha}_{3,k_1} - \hat{\alpha}_{3,k_1-L+1}) \theta^*, \\ \alpha_{3,i} &= \alpha_{3,k_1}, \quad i = k_1+1, \dots, k_1+M. \end{aligned} \quad (26)$$

Based on the pipeline features, the constraints on the attitude of the robot in the pipeline are determined. The constrained Euler angles of the robot are additional information for improving the accuracy of path reconstruction. Specifically, if the pipeline is built in horizontal planes with the standard pipe elbows except for a couple of pipes going up and down to avoid the obstacles, the above constraints on the Euler angles give the accurate attitude constraints for the robot in the pipeline, which can largely reduce the attitude and position errors of the robot.

### 3.2. Path reconstruction algorithm for the robot

The accurate path reconstruction for the robot can be completed by the technique of state estimation with state constraints [25]. The constraints on the Euler angles are regarded as the attitude measurements and the additional measurement equations for attitude can be established. Based on the constrained Euler angles (23)–(26), the corresponding attitude quaternion can be obtained by

$$q_k = \begin{bmatrix} \cos\left(\frac{\alpha_{3,k}}{2}\right) \cos\left(\frac{\alpha_{2,k}}{2}\right) \sin\left(\frac{\alpha_{1,k}}{2}\right) - \sin\left(\frac{\alpha_{3,k}}{2}\right) \sin\left(\frac{\alpha_{2,k}}{2}\right) \cos\left(\frac{\alpha_{1,k}}{2}\right) \\ \cos\left(\frac{\alpha_{3,k}}{2}\right) \sin\left(\frac{\alpha_{2,k}}{2}\right) \cos\left(\frac{\alpha_{1,k}}{2}\right) + \sin\left(\frac{\alpha_{3,k}}{2}\right) \cos\left(\frac{\alpha_{2,k}}{2}\right) \sin\left(\frac{\alpha_{1,k}}{2}\right) \\ \sin\left(\frac{\alpha_{3,k}}{2}\right) \cos\left(\frac{\alpha_{2,k}}{2}\right) \cos\left(\frac{\alpha_{1,k}}{2}\right) - \cos\left(\frac{\alpha_{3,k}}{2}\right) \sin\left(\frac{\alpha_{2,k}}{2}\right) \sin\left(\frac{\alpha_{1,k}}{2}\right) \\ \cos\left(\frac{\alpha_{3,k}}{2}\right) \cos\left(\frac{\alpha_{2,k}}{2}\right) \cos\left(\frac{\alpha_{1,k}}{2}\right) + \sin\left(\frac{\alpha_{3,k}}{2}\right) \sin\left(\frac{\alpha_{2,k}}{2}\right) \sin\left(\frac{\alpha_{1,k}}{2}\right) \end{bmatrix}, \quad (27)$$

The measurement of attitude error is given by

$$\delta\tilde{\alpha}_k = \begin{bmatrix} 2\mathbf{I}_3 & \mathbf{0}_{3 \times 1} \\ \mathbf{0}_{1 \times 3} & 0 \end{bmatrix} (\mathbf{q}_k \otimes \hat{\mathbf{q}}_k^{-1}), \quad (28)$$

where  $\otimes$  is quaternion multiplication. Then the additional measurement equation for the attitude error is given by

$$\delta\tilde{\alpha}_k = \delta\alpha_k + \mathbf{v}_k^c, \quad (29)$$

where  $\mathbf{v}_k^c$  is zero-mean Gaussian white noise with the covariance  $\mathbf{R}_k^c$  which avoids singular measurement noise covariance. Then, we obtain a new measurement matrix

$$\check{\mathbf{H}}_k = \begin{bmatrix} [(\mathbf{R}_n^b(\hat{\mathbf{q}}_k) \hat{\mathbf{v}}_k^n) \times] & \mathbf{0}_3 & \mathbf{R}_n^b(\hat{\mathbf{q}}_k) & \mathbf{0}_{3 \times 6} \\ \mathbf{I}_3 & \mathbf{0}_3 & \mathbf{0}_3 & \mathbf{0}_{3 \times 6} \end{bmatrix}, \quad (30)$$

and the measurement noise covariance

$$\check{\mathbf{R}}_k = \text{diag}(\mathbf{R}, \mathbf{R}_k^c). \quad (31)$$

Based on the pipeline features, the path reconstruction algorithm for the pipeline inspection robot is as follows:

a) State estimation for the system (1), (2), (6) and (9) using the EKF:

$$\mathbf{K}_k = \mathbf{P}_k^- \mathbf{H}_k^T (\mathbf{H}_k \mathbf{P}_k^- \mathbf{H}_k^T + \mathbf{R})^{-1}, \quad (32)$$

$$\mathbf{P}_k = (\mathbf{I} - \mathbf{K}_k \mathbf{H}_k) \mathbf{P}_k^-, \quad (33)$$

$$\delta\hat{\mathbf{x}}_k = \mathbf{K}_k \delta\mathbf{v}_{od,k}^b, \quad (34)$$

$$\hat{\mathbf{q}}_k = \hat{\mathbf{q}}_k^- + \frac{1}{2} \Xi(\hat{\mathbf{q}}_k^-) \delta\hat{\alpha}_k, \quad (35)$$

$$\hat{\mathbf{p}}_k = \hat{\mathbf{p}}_k^- + \delta\hat{\mathbf{p}}_k, \quad (36)$$

$$\hat{\mathbf{v}}_k^n = \hat{\mathbf{v}}_k^{n-} + \delta\hat{\mathbf{v}}_k^n, \quad (37)$$

$$\hat{\boldsymbol{\beta}}_{g,k} = \hat{\boldsymbol{\beta}}_{g,k}^- + \delta\hat{\boldsymbol{\beta}}_{g,k}, \quad (38)$$

$$\hat{\boldsymbol{\beta}}_{a,k} = \hat{\boldsymbol{\beta}}_{a,k}^- + \delta\hat{\boldsymbol{\beta}}_{a,k}. \quad (39)$$

The state prediction  $\hat{\mathbf{x}}_{k+1}^-$  is calculated based on (1), (2) and (6). The prediction error covariance is given by

$$\mathbf{P}_{k+1}^- = \mathbf{A}_k \mathbf{P}_k \mathbf{A}_k^T + \mathbf{G}_k \mathbf{Q} \mathbf{G}_k^T T_s. \quad (40)$$

The quaternion estimate  $\hat{\mathbf{q}}_k$  is obtained from (35).

b) Pipeline feature extraction and attitude constraint determination: with the quaternion estimate  $\hat{\mathbf{q}}_k$ , the pipeline features can be extracted based on the sliding window  $\{k-L+1, k\}$ . Accordingly, the attitude constraints at a certain time are determined by (23)–(26).

c) Path reconstruction for the robot: The EKF (32)–(40) is used again where  $\mathbf{H}_k$  and  $\mathbf{R}$  are replaced by  $\check{\mathbf{H}}_k$  and  $\check{\mathbf{R}}_k$ , respectively. The position estimates  $\hat{\mathbf{p}}_k$  from the obtained new state estimate  $\hat{\mathbf{x}}_k$  for all  $k$  are the reconstructed path for the robot and, consequently, the pipeline trajectory is determined.

The flowchart of the proposed trajectory determination method for pipelines using the inspection robot is shown in Fig. 2. The robot is put in the pipeline and the initial position, velocity and attitude of the robot are recorded. The robot moves through the pipeline and the data from the sensors on the robot are uploaded to a computer. The path reconstruction algorithm mentioned above is used to process the sensor data to estimate the motion of the robot. The trajectory of the pipeline is obtained based on the accurate position estimates of the robot.

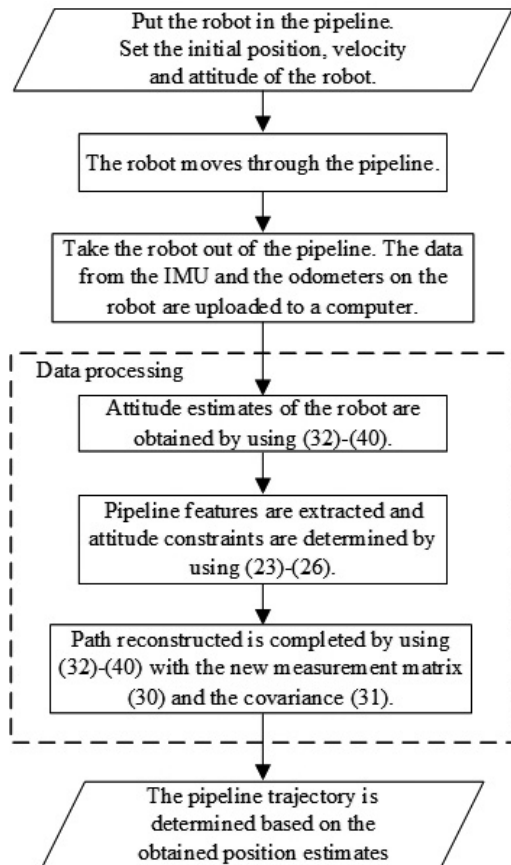


Fig. 2. Flowchart of the proposed method.

#### 4. Experiment

The accuracy of the proposed method should be evaluated in order to illustrate the advantage of the new method. Since the translation and rotation of the robot are constrained by the pipeline, it is difficult to accurately simulate the outputs of the accelerometer, the gyroscope and the odometers which reflect the motion of the robot in the pipeline, especially at its corners. Therefore, it is reasonable to evaluate the proposed method through an experimental study. First, a pipeline is built in the lab for the experiment, and, next, the robot runs in the pipeline. The data collected by the IMU and the odometers are used to determine the trajectory of the pipeline. The sensor data are shown in Fig. 3.

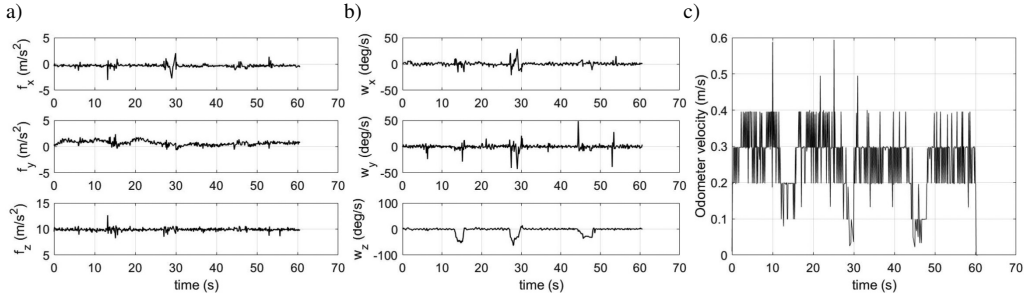


Fig. 3. Accelerometer data (a), gyroscope data (b) and odometer velocity (c).

Since GPS signal cannot be received in the lab, the four reference positions are set along the pipeline for analyzing the performance of the proposed method, as shown in Fig. 4(a). The grey rectangle represents the true trajectory of the pipeline. The time when the robot passes the reference positions are recorded. The position errors can be obtained by comparing the positions of the reconstructed path for the robot at the recorded time to the reference positions.

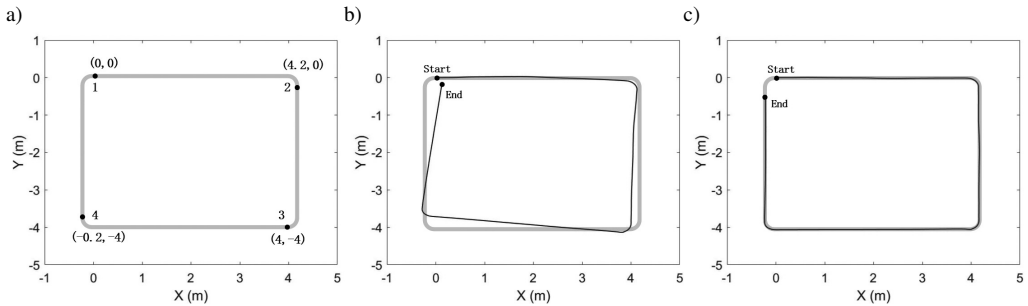


Fig. 4. Reference positions (a), trajectory determination using the standard EKF (b) and the proposed method (c).

Since it is inconvenient to represent the pipeline trajectory by latitudes and longitudes for the indoor experiment, the pipeline trajectory is obtained by integrating the velocity estimates. The pipeline trajectory determined by using a standard EKF with the IMU and odometer data is shown in Fig. 4(b). The black trajectory is the reconstructed path for the robot. The robot starts moving from the origin (reference position 1) toward right (1 → 2 → 3 → 4). The travel distance of the reconstructed path is close to the length of the pipeline, meaning that the odometer measurements were used in the EKF to reduce the travel distance error caused by accumulation of the accelerometer errors. Since the low-cost gyroscope cannot provide high-precision measurements of angular rate, the reconstructed path has relatively big orientation errors. Based on the reference positions in Fig. 4(a), the position errors of the reconstructed path for the robot are listed in Table 1.

The reconstructed path obtained by using the proposed method based on the pipeline features is shown in Fig. 4(c). The features of straight pipes are used to constrain the trajectory following a straight line, and the angles of the pipe elbows are used in the algorithm to make the trajectory turn 90 degrees at each corner. Compared to the trajectory in Fig. 4(b), the proposed method has much better performance than the standard EKF. The reconstructed path in Fig. 4(c) almost coincides with the true trajectory of the pipeline. The position errors of the reconstructed path

Table 1. Position error of using the standard EKF.

| Reference position | $\Delta X$ [m] | $\Delta Y$ [m] | $\sqrt{\Delta X^2 + \Delta Y^2}$ [m] |
|--------------------|----------------|----------------|--------------------------------------|
| 1                  | 0              | 0              | 0                                    |
| 2                  | 0.0775         | 0.1015         | 0.1277                               |
| 3                  | 0.2268         | 0.1299         | 0.2614                               |
| 4                  | 0.0793         | -0.3886        | 0.3966                               |

are listed in Table 2. It can be seen in Tables 1 and 2 that the position errors significantly reduce by using the proposed method because the pipeline features provide constraints on the attitude of the robot, which is used to correct the attitude and position errors of the robot caused by the measurement errors of the low-cost IMU. The position errors in Table 2 are less than 40% of the corresponding position errors in Table 1.

Table 2. Position error of using the proposed method.

| Reference position | $\Delta X$ [m] | $\Delta Y$ [m] | $\sqrt{\Delta X^2 + \Delta Y^2}$ [m] |
|--------------------|----------------|----------------|--------------------------------------|
| 1                  | 0              | 0              | 0                                    |
| 2                  | 0.0424         | 0.0272         | 0.0504                               |
| 3                  | 0.0259         | -0.0214        | 0.0336                               |
| 4                  | 0.0233         | 0.0343         | 0.0415                               |

The experiment results show the effectiveness and advantage of the proposed pipeline trajectory determination method. By introducing the pipeline features, the accurate trajectory can be obtained by using the new path reconstruction algorithm even if a low-cost chip based IMU is used on the pipeline inspection robot, which significantly improves the performance of pipeline trajectory determination.

Although the proposed method has much better performance compared to the standard EKF, there still are slowly accumulating position errors if the number of turns and travel distance increases, especially in a long-distance application. Standard angles of the pipe elbows are used as additional measurements to improve the accuracy of the reconstructed trajectory. However, in practice, the actual turn angle of the pipeline is a little different from the standard angle of the elbow because of machining errors and installation errors. On the other hand, the wheels of the odometers slip if there is dust or oil on the wall of the pipeline, leading to increased travel distance error of the reconstructed trajectory in a long-distance application. In order to improve accuracy in a long-distance application, the above ground marks are used to correct the position errors. With the advantage of the proposed method, fewer above ground marks are needed to reach a good performance of trajectory determination for a long-distance pipeline.

## 5. Conclusions

In this paper, a new trajectory determination method is proposed for pipelines using an inspection robot. The low-cost MEMS based IMU and odometers are applied on the robot for collecting motion information when the robot runs in a pipeline. The kinematic model and measurement model are created for estimating the position, velocity and attitude of the robot. The

error propagation model is derived for compensating estimate errors. The path reconstruction algorithm is proposed to obtain pipeline features and complete trajectory determination based on sensor data from the IMU and odometers. An experiment is conducted to illustrate the effectiveness and advantage of the proposed method. In the future, the proposed trajectory determination method will be applied in outdoor experiments.

## Acknowledgement

This work was supported by the Canada Mitacs Elevate Postdoctoral Fellowship Program (grant # IT15728).

## References

- [1] Liu, Z., & Kleiner, Y. (2013). State of the art review of the inspection technologies for condition assessment of water pipes. *Measurement*, 46(1), 1–15. <https://doi.org/10.1016/j.measurement.2012.05.032>
- [2] Kishawy, H. A., & Gabbar, H. A. (2010). Review of pipeline integrity management practices. *International Journal of Pressure Vessels and Piping*, 87(7), 373–380. <https://doi.org/10.1016/j.ijpvp.2010.04.003>
- [3] Zhang, T., Wang, X., Chen, Y., Shuai, Y., Ullah, Z., Ju, H., & Zhao, Y. (2019). Geomagnetic detection method for pipeline defects based on ceemdan and WEP-TEO. *Metrology and Measurement Systems*, 26(2), 345–361. <https://doi.org/10.24425/mms.2019.128363>
- [4] Ju, H., Wang, X., Zhang, T., Zhao, Y., & Ullah, Z. (2019). Defect recognition of buried pipeline based on approximate entropy and variational mode decomposition. *Metrology and Measurement Systems*, 26(4), 735–755. <https://doi.org/10.24425/mms.2019.129587>
- [5] Piao, G., Guo, J., Hu, T., & Deng, Y. (2019). High-sensitivity real-time tracking system for high-speed pipeline inspection gauge. *Sensors*, 19(3), 731. <https://doi.org/10.3390/s19030731>
- [6] De Araújo, R. P., De Freitas, V. C. G., De Lima, G. F., Salazar, A. O., Neto, A. D. D., & Maitelli, A. L. (2018). Pipeline inspection gauge's velocity simulation based on pressure differential using artificial neural networks. *Sensors*, 18(9), 3072. <https://doi.org/10.3390/s18093072>
- [7] Chowdhury, M. S., & Abdel-Hafez, M. F. (2016). Pipeline inspection gauge position estimation using inertial measurement unit, odometer, and a set of reference stations. *ASCE-ASME Journal of Risk and Uncertainty in Engineering Systems Part B: Mechanical Engineering*, 2(2), 021001-1-10. <https://doi.org/10.1115/1.4030945>
- [8] Coramik, M., & Ege, Y. (2017). Discontinuity inspection in pipelines: a comparison review. *Measurement*, 111, 359–373. <https://doi.org/10.1016/j.measurement.2017.07.058>
- [9] Idroas, M., Abd Aziz, M. F. A., Zakaria, Z., & Ibrahim, M. N. (2019). Imaging of pipeline irregularities using a PIG system based on reflection mode ultrasonic sensors. *International Journal of Oil, Gas and Coal Technology*, 20(2), 212–223. <https://doi.org/10.1504/IJOGCT.2019.097449>
- [10] Li, Z., Wang, J., Li, B., & Gao, J. (2014). GPS/INS/Odometer integrated system using fuzzy neural network for land vehicle navigation. *Journal of Navigation*, 67(6), 967–983. <https://doi.org/10.1017/S0373463314000307>
- [11] Jiang, Q., Wu, W., Jiang, M., & Li, Y. (2017). A new filtering and smoothing algorithm for railway track surveying based on landmark and IMU/odometer. *Sensors*, 17(6), 1438. <https://doi.org/10.3390/s17061438>

- [12] Georgy, J., Karamat, T., Iqbal, U., & Noureldin, A. (2011). Enhanced MEMS-IMU/odometer/GPS integration using mixture particle filter. *GPS Solutions*, 15(3), 239–252. <https://doi.org/10.1007/s10291-010-0186-4>
- [13] Zhao, Y. (2015) Cubature plus extended hybrid Kalman filtering method and its application in PPP/IMU tightly coupled navigation systems. *IEEE Sensors Journal*, 15(12), 6973–6985. <https://doi.org/10.1109/JSEN.2015.2469105>
- [14] Guan, L., Cong, X., Zhang, Q., Liu, F., Gao, Y., An, W., & Noureldin, A. (2020). A comprehensive review of micro-inertial measurement unit based intelligent PIG multi-sensor fusion technologies for small-diameter pipeline surveying. *Micromachines*, 11(9), 840. <https://doi.org/10.3390/mi11090840>
- [15] Wang, L., Wang, W., Zhang, Q., & Gao, P. (2014). Self-calibration method based on navigation in high-precision inertial navigation system with fiber optic gyro. *Optical Engineering*, 53(6), 064103. <https://doi.org/10.1117/1.OE.53.6.064103>
- [16] Usarek, Z., & Warnke, K. (2017). Inspection of gas pipelines using magnetic flux leakage technology. *Advances in Materials Science*, 17(3), 37–45. <https://doi.org/10.1515/adms-2017-0014>
- [17] Sasani, S., Asgari, J., & Amiri-Simkooei, A. R. (2016). Improving MEMS-IMU/GPS integrated systems for land vehicle navigation applications. *GPS solutions*, 20(1), 89–100. <https://doi.org/10.1007/s10291-015-0471-3>
- [18] Hyun, D., Yang, H. S., Park, H. S., & Kim, H. J. (2010). Dead-reckoning sensor system and tracking algorithm for 3-D pipeline mapping. *Mechatronics*, 20(2), 213–223. <https://doi.org/10.1016/j.mechatronics.2009.11.009>
- [19] Lee, D. H., Moon, H., Koo, J. C., & Choi, H. R. (2013). Map building method for urban gas pipelines based on landmark detection. *International Journal of Control, Automation, and Systems*, 11(1), 127–135. <https://doi.org/10.1007/s12555-012-0049-6>
- [20] Li, T., Zhang, H., Niu, X., & Gao, Z. (2017). Tightly-coupled integration of multi-GNSS single-frequency RTK and MEMS-IMU for enhanced positioning performance. *Sensors*, 17(11), 2462. <https://doi.org/10.3390/s17112462>
- [21] Sahli, H., & El-Sheimy, N. (2016). A novel method to enhance pipeline trajectory determination using pipeline junctions. *Sensors*, 16(4), 567. <https://doi.org/10.3390/s16040567>
- [22] Guan, L., Cong, X., Sun, Y., Gao, Y., Iqbal, U., & Noureldin, A. (2017). Enhanced MEMS SINS aided pipeline surveying system by pipeline junction detection in small diameter pipeline, *IFAC-PapersOnLine*, 50(1), 3560–3565. <https://doi.org/10.1016/j.ifacol.2017.08.962>
- [23] Crassidis, J. L., & Junkins, J. L. (2011). *Optimal Estimation of Dynamic Systems*. CRC press. <https://doi.org/10.1201/b11154>
- [24] Noureldin, A., Karamat, T. B., & Georgy, J. (2012). *Fundamentals of Inertial Navigation, Satellite-Based Positioning and their Integration*. Springer Science & Business Media. <https://doi.org/10.1007/978-3-642-30466-8>
- [25] Xu, L., Li, X. R., Duan, Z., & Lan, J. (2013). Modeling and state estimation for dynamic systems with linear equality constraints. *IEEE Transactions on Signal Processing*, 61(11), 2927–939. <https://doi.org/10.1109/TSP.2013.2255045>



**Shuo Zhang** received the Ph.D. degree from Beihang University, China, in 2016. He worked as a postdoctoral fellow at Tsinghua University, China, from 2016 to 2019. He is currently a Mitacs postdoctoral fellow with the Department of Chemical and Materials Engineering, University of Alberta, Edmonton, AB, Canada. His research interests include optimal estimation, multi-sensor fusion, navigation, and signal processing with applications

to biomedical engineering.



**Stevan Djuljevic** received the Ph.D. degree from the Henry Samueli School of Engineering and Applied Science, University of California at Los Angeles (UCLA), Los Angeles, CA, USA, in 2005. He is currently Associate Professor with the Department of Chemical and Materials Engineering, University of Alberta, Edmonton, AB, Canada. His research interests include systems engineering, with the emphasis on model predictive control of distributed param-

eter systems, dynamics and optimization of material and chemical process operations, computational modeling and simulation of biological systems (cardiac electrophysiological systems), and biomedical engineering.